Radiative cooling instabilities in the low dense plasma corona of laserirradiated solid targets

L. J. Dhareshwar, P. A. Naik, Susmita Sarkar, Manoranjan Khan, and B. Chakraborty

Citation: Physics of Fluids B: Plasma Physics (1989-1993) **4**, 1635 (1992); doi: 10.1063/1.860072
View online: http://dx.doi.org/10.1063/1.860072
View Table of Contents: http://scitation.aip.org/content/aip/journal/pofb/4/6?ver=pdfcov
Published by the AIP Publishing

Radiative cooling instabilities in the low dense plasma corona of laser-irradiated solid targets

L. J. Dhareshwar and P. A. Naik
Laser Division, Bhabha Atomic Research Centre, Bombay 400085, India

Susmita Sarkar,[a] Manoranjan Khan, and B. Chakraborty
Plasma Physics Group, Department of Mathematics, Faculty of Science, Jadavpur University, Calcutta 700 032, India

(Received 11 March 1991; accepted 10 February 1992)

Plasma jets produced from targets with atomic numbers ranging from 5 to 82 have been investigated in detail. Theoretical modeling based on a radiative cooling instability has been used to successfully explain the experimental results. Optical shadowgrams and x-ray pinhole pictures strongly indicate a correlation between the jets and x-ray emission from plasma. Plasma jets are intense in materials such as copper, molybdenum, tungsten, and gold which are characterized by strong x-ray emission. Interferograms indicate a large increase in electron density in the region of plasma jets.

I. INTRODUCTION

Optical[1,2] and x-ray[3,4] probing of laser-irradiated targets have often revealed the breakup of plasma into thin filamentary jetlike structures. Our earlier experimental observations[5] have also helped us to get a qualitative picture of plasma jets. It has been observed that though plasma jets appear similar to the density structures produced due to laser beam filamentation in underdense plasma, they have been found to have distinctly different characteristics. A close examination of plasma jets shows that they lie outside the cone angle of the laser beam[5,6] unlike filaments that are confined to the laser beam region.[7] The plasma jets are not along the laser beam but follow the plasma flow direction.[8] It has also been observed that plasma jetting is more pronounced after the laser pulse is over and therefore has no effect on the hydrodynamic stability of the accelerated foil targets.[5] Unlike filaments, plasma jets appear at laser intensities as low as 10^{11} W/cm^2 and have no relevance either to laser beam or target nonuniformities. It has been reported that plasma jetting is enhanced at shorter wavelengths[6,8] and for target materials with higher atomic numbers.[5,6] It, therefore, seems that the physical mechanisms responsible for laser beam filamentation and plasma jetting are quite different. Ponderomotive force[9] or differential heating[10] of plasma in the regions of higher laser intensity can cause laser beam filamentation to occur. Therefore, the typical threshold for laser beam filamentation is higher than 10^{13} W/cm^2. The most recent experimental results presented by Gabl *et al.*[11] have shown that plasma jets are cold with respect to the background plasma and move faster. In the indirect-drive inertial confinement fusion scheme, the implications of such plasma jets could be serious. A nonuniform expansion of the high-density plasma from the gold cavity could result in an implosion nonuniformity. Even in the direct-drive scheme, if the jets grow considerably during the initial part of the laser pulse, then laser beam refraction due to jets could result in a nonuniform illumination at the target. Achievement of laser action in the x-ray region using laser-produced plasmas as gain media has assumed considerable importance in recent years. In these schemes, formation of plasma jets would disturb the conditions of plasma to get optimum x-ray lasing. The influence of plasma jets on x-ray laser schemes have been discussed by Xu and co-workers.[12,13]

The formation of plasma jets in certain laser-irradiated targets was first theoretically studied by Evans[14] using the radiation cooling instability model. The experimental observations discussed in this paper strongly suggest the possibility of the radiative type of a cooling instability to occur under certain conditions in a laser-produced plasma. The conditions necessary for the growth of such an instability are associated with optically thin radiative losses from the plasma. When the plasma is in a state that the local heating rate is a weak function of local density and temperature and also balanced by optically thin radiative losses, then any local density fluctuation can give rise to the instability. In such a condition, an increase in the local density results in an increased radiative loss which causes a reduction of temperature and kinetic pressure of plasma. The surrounding plasma is thus pushed into this region and the instability starts growing. This causes the breakup of the ablating plasma into jetlike structures. In addition, several explanations such as an electrothermal[15] and a magnetothermal[16] instability have been proposed earlier.

In our present work conducted with 11 elements whose atomic numbers vary from 5 to 82, the most striking observations are a strong dependence of plasma jetting on the x-ray emission from the plasma which has not been hitherto shown explicitly. X-ray pinhole pictures of the plasma plume indicate enhanced x-ray emission from the region of plasma jets. Time-resolved interferograms of these targets show a 5–10 time enhancement of plasma density in the region of jets as compared to the rest of the background plasma. The plasma jets have been found to be present in the

[a] Permanent address: Department of Mathematics, University of Burdwan, Burdwan 713104, India.

 0899-8221/92/061635-08$04.00

plasma even as late as 12 nsec after the irradiation by the laser pulse. In the case of thin foil targets it has been observed that jets appear even on the rear side of the thin foil. In addition, several other interesting features relating to the plasma jets will be presented in this paper. Section II discusses the analytical model based on a radiative type of cooling instability. Section III discusses the details of experiments and Sec. IV contains results and a comparison with the theoretical model. Conclusions are included in Sec. V.

II. THEORETICAL MODEL

As discussed in the Introduction, the earlier results by several laboratories as well as our results presented in Secs. III and IV strongly indicate the growth of plasma jets due to a radiative cooling type instability set up in the plasma corona. Before discussing the rigorous model, the following argument has also been used to explain some of the observations. Since the radiative cooling instability arises due to enhanced radiative losses from regions of enhanced local density, it can be characterized by three time scales, namely the radiative cooling time τ_R, thermal conduction time $\tau_{\rm th}$, and the sound transit time τ_s which is the typical time scale over which plasma is pushed into the jet region. It can be simply visualized that the condition for the growth of a radiative cooling instability is that $\tau_R \ll \tau_{\rm th}$ and τ_s and also $\tau_s < \tau_{\rm th}$. This condition takes care that the density perturbations are not smoothed out by classical thermal conduction. In practical situations, τ_R is always much less than either $\tau_{\rm th}$ or τ_s. However, if thermal conduction is large so that $\tau_{\rm th} \ll \tau_s$, the density perturbations are not simply smoothed since density perturbations still exist due to acoustic waves. An order of magnitude estimate of the values of these time scales in order that a jet of dimension of 50 μm can grow can be done considering a self-regulating model for plasma expansion.[17] This model can be considered valid for an irradiation pulse duration of a few nanoseconds, as in the present case, and also considering only bremsstrahlung emission. Therefore, from

$$\tau_R = \frac{\text{Plasma energy in region of jet}}{\text{Energy radiated per second}},$$

and considering a typical coronal density of $10^{20}\ \text{cm}^{-3}$ and a coronal temperature of 100 eV for a gold plasma at incident laser intensity in the range of 5×10^{12} to $10^{13}\ \text{W/cm}^2$, calculations show that $\tau_R \simeq 10^{-13}$ sec. A typical ion sound speed is given by the expression[17]

$$c_s = 3\times10^7[(Z/A)^{1/2}(T_e/1\ \text{keV})^{1/2}].$$

Therefore $\tau_s = (d/c_s) \simeq 0.5\times10^{-9}$ sec. In this calculation, d is the scale length of density nonuniformity (diameter of the jet) and is taken as 50 μm.

The classical thermal conduction time calculated by using Spitzer's conductivity formula as used by Dawson[18] is given by the expression

$$\tau_{\rm th} = 2n_e(Z+1)10^{-28}(\ln\Lambda)d^2/5.85T^{5/2},$$

where n_e = electron density (electrons per cm^3), Z = atomic number, and T = temperature (in keV).

Substituting values for T, n_e, d, $\ln\Lambda \simeq 10$, $T = 0.1$ keV, and $Z \simeq 19$ for gold at this temperature,[17] therefore, $\tau_{\rm th} \simeq 10^{-9}$ sec. These estimates show that with the values of $\tau_{\rm th}$ and τ_s being so close, there exists a narrow range of values of d for which possibly the instability can grow. In the limit $\tau_s \gtrsim \tau_{\rm th}$, therefore, temperature and density fluctuations both assume importance. A detailed analytical modeling of the instability growth is given below.

Following Evans, the idea has been quantitatively developed by considering an equilibrium in which the source energy $S(\text{Wkg}^{-1})$ is balanced by a radiative loss term $R(\text{Wkg}^{-1})$, where S and R are assumed to vary with density and temperature as

$$S = S_0(\rho/\rho_0)^{\alpha_1}(T/T_0)^{\alpha_2}, \tag{1}$$

$$R = R_0(\rho/\rho_0)^{\beta_1}(T/T_0)^{\beta_2}, \tag{2}$$

where ρ_0 and T_0 are equilibrium values, so that $S_0 = R_0$. The exponents α_1 and α_2 depend upon the laser absorption process, whereas β_1 and β_2 depend upon the radiation process.

The basic equations describing this problem are energy, mass, and momentum balance equations. The plasma is assumed to be a perfect gas satisfying the following expressions for the equation of state:

$$p = (\bar{Z}+1)n_iK_BT,$$

$$\epsilon = (\tfrac{3}{2})p, \quad \rho_i = n_im_i, \tag{3}$$

where $\bar{Z}$ is the effective charge of the ions, K_B is the Boltzmann constant, n_i is the density of ions per unit volume, T is the plasma temperature, ϵ is the plasma expansion energy, and m_i is the ion mass.

The linearized dispersion relation in this problem has the form

$$F(\gamma) = \gamma^3\left(\frac{\epsilon_0}{\rho_0}\right) + \gamma^2\left(\frac{K^2\varkappa_0}{\rho_0}T_0 + R_0(\beta_2-\alpha_2)\right) + \gamma\left(\frac{5}{2}\frac{K^2p_0^2}{\rho_0^2}\right) + \frac{K^2p_0}{\rho_0}\left(\frac{K^2\varkappa_0}{\rho_0}T_0 + R_0[(\beta_2-\alpha_2)-(\beta_1-\alpha_1)]\right) = 0, \tag{4}$$

where $\varkappa_0$ is the thermal conductivity, γ the growth rate, and K the wave number for the density perturbation. The above equation has at least one positive real root if

$$(K^2\varkappa_0/\rho_0)T_0 + R_0[(\beta_2-\alpha_2)-(\beta_1-\alpha_1)] < 0 \tag{5}$$

or

$$R_0 > (K^2\varkappa_0/\rho_0)T_0/[(\alpha_2-\beta_2)-(\alpha_1-\beta_1)], \tag{6}$$

provided $(\alpha_2-\beta_2) > (\alpha_1-\beta_1)$. This type of instability can be termed an absolute instability.

Other than the absolute instability, another type of instability can grow when the dispersion relation has no positive real root but contains a pair of complex roots with positive real parts. Such instability is known as convective instability. Using Routh criteria[19] we have observed that the convective instability occurs if

$$R_0 > (K^2\varkappa_0/\rho_0)T_0/(\alpha_2-\beta_2) \tag{7}$$

for $\alpha_2 > \beta_2$. Below this threshold convective instability may also grow if

$$R_0 > (K^2\kappa_0/\rho_0)T_0/[(\alpha_2-\beta_2)+\tfrac{3}{2}(\alpha_1-\beta_1)], \quad (8)$$

provided

$$(\alpha_2-\beta_2)+\tfrac{3}{2}(\alpha_1-\beta_1)>0. \quad (9)$$

Since for $\alpha_1>\beta_1$, the right-hand side of (8) is less than that of (7), convective instability develops if the inequality (8) holds. Thus, absolute instability occurs if the inequality (6) holds and convective instability occurs if

$$(K^2\kappa_0/\rho_0)T_0/[(\alpha_2-\beta_2)+\tfrac{3}{2}(\alpha_1-\beta_1)] < R_0 < (K^2\kappa_0/\rho_0)T_0/[(\alpha_2-\beta_2)-(\alpha_1-\beta_1)]. \quad (10)$$

We may thus conclude that when R_0 exceeds the value

$$(K^2\kappa_0/\rho_0)T_0/[(\alpha_2-\beta_2)+\tfrac{3}{2}(\alpha_1-\beta_1)],$$

the convective instability grows but it is dominated by the absolute instability when R_0 becomes equal to

$$(K^2\kappa_0/\rho_0)T_0/[(\alpha_2-\beta_2)-(\alpha_1-\beta_1)].$$

Since the thermal conductivity κ_0 is inversely proportional to the ion charge Z, from inequalities (6) and (8) it is clear that the threshold value of the radiation loss decreases for high-Z mateials and also decreases for smaller values of the wave number K. Thus for high-Z targets[20,21] more pronounced jetting is expected. Larger jet dimensions which are characterized by lower K values can be expected to be seen at lower thresholds or at lower laser intensities. The higher K values having a higher threshold can thus be expected at higher laser intensities. After the laser pulse absolute instability could occur if inequality (6) holds. Moreover, since the right-hand side of inequality (8) is less than that of (7) convective instability occurs if

$$(K^2\kappa_0/\rho_0)T_0/[(\alpha_2-\beta_2)+\tfrac{3}{2}(\alpha_1-\beta_1)] < R_0 < (K^2\kappa_0/\rho_0)T_0/[(\alpha_2-\beta_2)-(\alpha_1-\beta_1)].$$

Inequalities (6) and (10) show that occurrence of absolute instability and convective instability are two mutually exclusive events within the range of the radiation loss specified above.

In a specific experimental situation, to obtain the dimension d of the jet we have to find the value of the wave number K for which the growth rate γ is maximum and satisfies the equation

$$d\gamma/dK = 0. \quad (11)$$

Differentiating Eq. (4) with respect to K and substituting (11) we obtain the quadratic equation

$$\gamma_m^2(\kappa_0T_0\rho_0)+\gamma_m(\tfrac{5}{2}p_0^2)+2K^2\kappa_0T_0p_0 + R_0p_0\rho_0[(\beta_2-\alpha_2)-(\beta_1-\alpha_1)]=0, \quad (12)$$

which is satisfied by the maximum growth rate γ_m. This maximum growth rate should be real and positive if the wave number K satisfies

$$2K^2\kappa_0T_0p_0+R_0p_0\rho_0[(\beta_2-\alpha_2)-(\beta_1-\alpha_1)]<0$$

or wave number

$$K<\left(\frac{R_0\rho_0}{2\kappa_0T_0}[(\beta_1-\alpha_1)-(\beta_2-\alpha_2)]\right)^{1/2}. \quad (13)$$

The corresponding wavelength λ' is therefore given by

$$\lambda' = 2\pi/K > 2\pi\{(R_0\rho_0/2\kappa_0T_0)[(\beta_1-\alpha_1)-(\beta_2-\alpha_2)]\}^{-1/2}. \quad (14)$$

Since the diameter of the jet d must exceed λ' we have

$$d\geqslant\lambda' > 2\pi\{(R_0\rho_0/2\kappa_0T_0)[(\beta_1-\alpha_1)-(\beta_2-\alpha_2)]\}^{-1/2}. \quad (15)$$

This equation gives a threshold value of the jet diameter.

The values of α_1 and α_2 depend upon the process of absorption whereas the values of β_1 and β_2 depend exclusively on the radiation process. Normally, the laser energy is absorbed by processes like inverse bremsstrahlung, resonant absorption, two plasmon decay, etc. In the experiment discussed above conducted with Nd:glass laser intensity $\simeq 5\times10^{12}$ W/cm^2, the plasma formed in most of the materials is highly collisional and energy absorption possibly occurs mostly by inverse bremsstrahlung, for which we can choose $\alpha_1=1$, $\alpha_2=-3/2$, and for all radiation processes $\beta=1$. Therefore from (6) and (9) it is clear that instability occurs for $\beta_2<-3/2$. In the experiments conducted with low-z targets, such as Zapon which are fully ionized, radiation loss through free–free bremsstrahlung dominates over other radiation processes. But copper is a moderate-z target, having $\bar{z}=16$, and the radiation process is partly free–free bremsstrahlung and partly free–bound and bound–bound process. For high-z ($=79$) targets, like gold having $\bar{z}\simeq23$, the plasma is partially ionized and the bound–bound radiation process dominates over other processes.

In the case of the rear side of the target where the jets are also observed, the instability can be understood from a typical numerical estimation done for a copper target. In this region typically $T_e\simeq10$ eV, from experiments $K=1.2\times10^3$/cm, $n_e=0.8\times10^{18}$/cm^3, $\bar{z}=2.6$, $\kappa_0=3.2\times10^6$ ergs/(sec deg cm). Since on the rear side there is no laser energy source, we can consider $\alpha_1=\alpha_2=0$. Also, since energy is radiated mostly by free–free bremsstrahlung, we can substitute $\beta_1=1$, $\beta_2=1/2$. Thus absolute instability occurs in the plasma since $\alpha_2-\beta_2=-1/2$, which is greater than $\alpha_1-\beta_1=-1$, and plasma jets will be observed on the rear side of the target.

III. EXPERIMENTS

Experiments were conducted with the Nd:glass laser amplifier chain delivering 20 J energy in a pulse of duration 5 nsec (full width at half-maximum). Several diagnostics have been used to study the evolution of plasma jets. The schematic experimental arrangement is shown in Fig. 1. For optical shadowgraphy and interferometry, the second-harmonic optical probe beam used was generated by splitting a fraction of the main laser beam which ensured the self synchronization of the probe pulse with the main pulse. After splitting, the probe beam was frequency up-converted using a type-1 phase matched KDP crystal with a 3% conversion efficiency. A KG3 filter was used to cut off the residual 1.06 μm beam. A spatial filter incorporated in the path of the probe beam ensured a uniform spatial profile. The second-harmonic probe pulse duration was reduced to 1–1.5 nsec to achieve

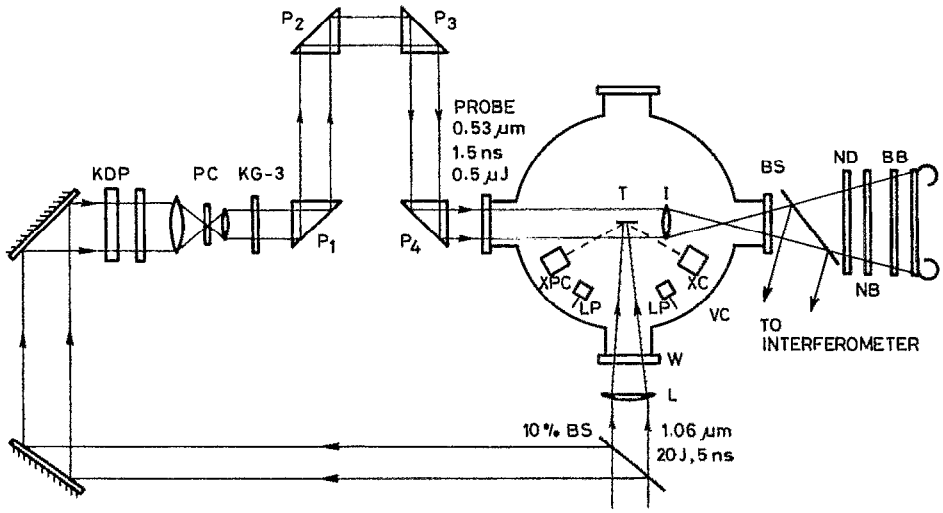

FIG. 1. Schematic of the experiment to record optical shadowgrams and x-ray pinhole pictures of the plasma corona. T: target; L: focusing lens; W: window of vacuum chamber (Vc); I: imaging optics; XPC: x-ray pinhole camera; ND, NB: neutral density and narrow-band 0.53 mm green filters to cut off plasma luminosity; C: Polaroid camera; BS: beamsplitter; XC: x-ray calorimeter; LP: Langmuir probe; KDP: crystal to produce second-harmonic probe beam; PC: probe pulse shortening device; KG3: filter to cut off residual 1.06 μm laser beam; P_1, P_2, P_3, and P_4: beam folding prisms of the variable optical delay.

a good temporal resolution. The probe beam was incident on the target as indicated in Fig. 1. For optical shadowgraphy, the target was imaged using an $f/3.5$ lens with a $15\times$ magnification on Polaroid film of speed 3000 ASA. The spatial resolution of this optical imaging system was 6 μm. A broadband green filter of Schott BG-18 glass and a narrow-band filter with center transmission wavelength at 0.53 μm were used to suppress plasma luminosity. An optical delay in the path of the probe beam variable in the range of 10–12 nsec could be used to obtain plasma shadowgrams and interferograms at various instants of time with respect to the peak of the main laser pulse. Optical interferograms were obtained by using a lateral shearing type of interferometer. This type of interferometer could give plasma interferograms as well as shadowgrams simultaneously. This was helpful since the shadowgrams could be used to locate plasma jets and interferograms showed the density variations in the region of the jets.

The relative x-ray emission from the different targets was measured using an x-ray PIN detector of type 100-N-125. A 25 μm thick beryllium filter was used with this detector to detect photon energies above 1 keV. The electric voltage pulse height was displayed on a digital pulse height detector. Differential x-ray calorimeters also have been used to measure the x-ray emission from different targets. These calorimeters consisted of two 6 μm thick, 5 mm diam tantalum disks on the rear side of which Chromel-constant thermocouples were welded. One disk was covered with a quartz plate to detect only scattered laser radiation and the other was covered with a 1–2 μm thick plastic foil which transmitted x-ray laser radiation. Thus, the net voltage generated across the thermocouple array was proportional to the x-ray energy incident on one of the tantalum disks. Plasma expansion velocity was measured using a Langmuir probe. X-ray pinhole pictures of the plasma plume were recorded using a 25 μm diam pinhole on Kodak DEF-5 x-ray film. Magnification of the pinhole camera was $5\times$ and spatial resolution was about 25 μm.

The laser beam was focused on the targets using an $f/5$ lens of 50 cm focal length. The minimum diameter of the laser spot at the beam waist was 65 μm. However, experiments were conducted with 160 and 350 μm spot diameters also, which were produced by moving the target plane into the near field of the lens. Targets used were thin foils as well as massive targets. The targets are described in Table I.

IV. RESULTS AND DISCUSSIONS

Optical shadowgrams for zapon, aluminum, titanium, gold, and lead are shown, respectively, in Figs. 2(a)–2(e). It can be clearly observed that whereas plasma jets are totally

TABLE I. Target materials used in the experiments.

Target material	Atomic number	Foil thickness (microns)
Zapon($C_6H_7O_{11}N_3$)	5.6 (avg)	10
Magnesium	12	100
Aluminum	13	6
Titanium	22	12
Copper	29	10
Molybdenum	42	25
Tin	50	50
Tantalum	73	8
Tungsten	74	25
Gold	79	40

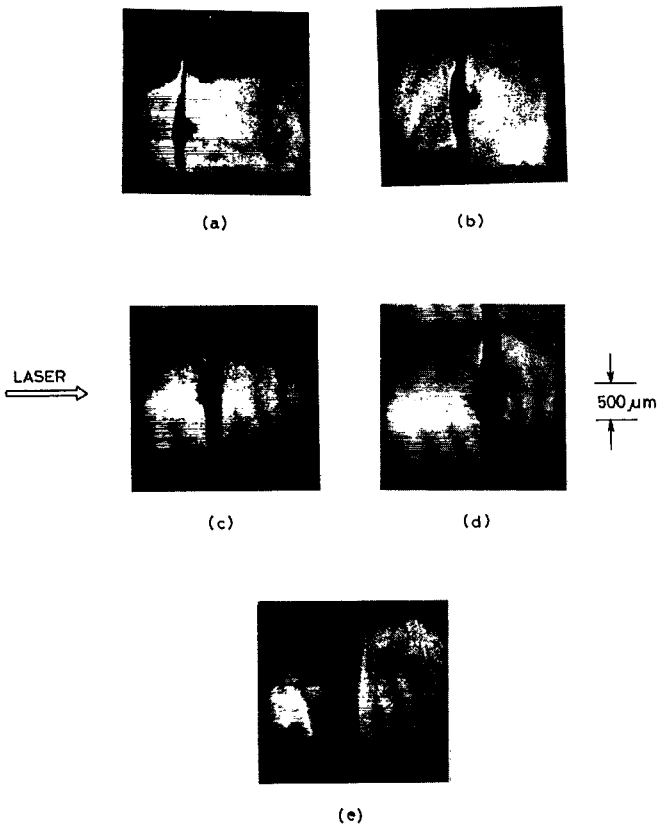

FIG. 2. Optical shadowgrams for (a) zapon, (b) aluminum, (c) titanium, (d) gold, and (e) lead. Laser intensity = 5×10^{12} W/cm^2, optical probe delay = 7 nsec with respect to peak of the main laser beam.

absent in zapon and aluminum, in the other materials plasma jetting is present to a varying extent. Quantitatively, the extent of plasma jetting in varying atomic number targets was defined by the jet density or the number of plasma jets per unit length. The plasma jet density was measured by determining the average jet diameter d of many jets at a fixed distance from the target surface. A normalized value of $1/d$ was defined thus as the jet density. The justification for the choice of such a parmeter can be understood by considering the growth of the radiation cooling instability as explained by Evans.[14] If in the coronal region after the laser pulse the plasma is optically thin to its radiative losses, then any local enhancement in plasma density leads to an increased radiative loss. This is followed by a reduction in temperature and plasma pressure, resulting in plasma from neighboring regions being pushed into this region, thus increasing plasma density in the region of the jets. Thus the instability can grow causing high plasma density jet regions. The plasma jet growth and the fastest growing jet frequency are decided by radiation cooling rate, thermal conduction lengths, and the rate at which plasma moves into the jet regions, which is decided by the sound transit time and therefore depends upon laser intensity. Thus at a given distance from the target, the jet growth rate is fixed. Since the plasma jets are observed to be fairly uniformly distributed over the plasma diameter, the ratio of number of jets to plasma diameter at a fixed distance from the target is a good quantitative estimate of the extent of jetting for a given material. Figure 3 shows the plot (a) of normalized values of $1/d$ versus target atomic number and (b) shows the plot of relative radiation losses from

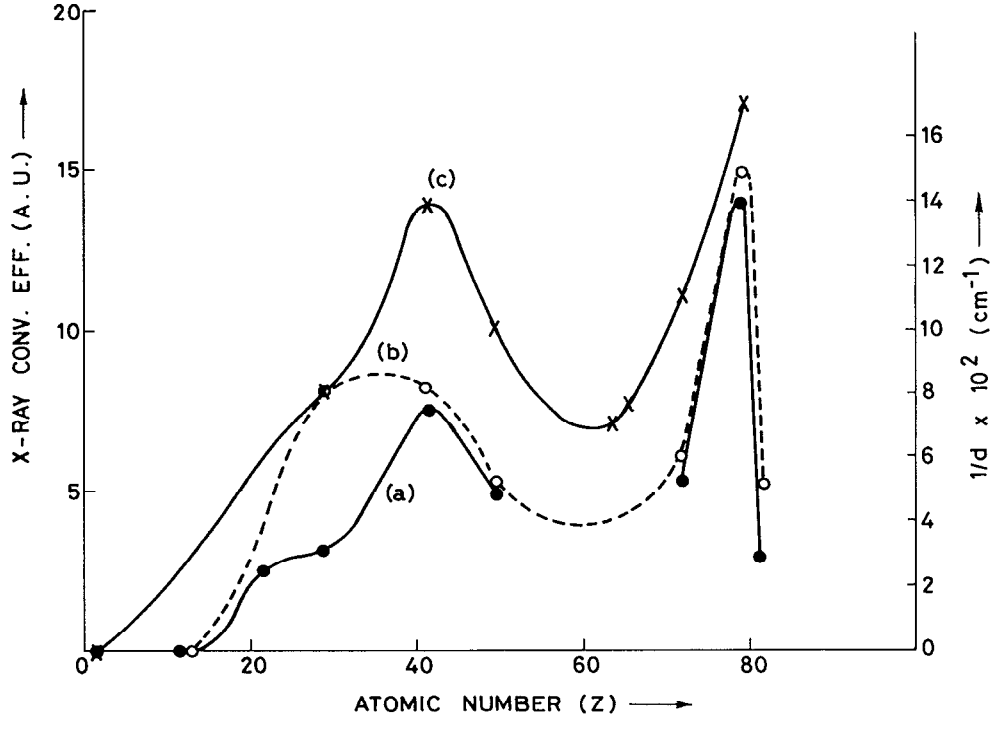

FIG. 3. Plot of (a) normalized values of $1/d$ (d is the average jet diameter) against target atomic number, (b) normalized measured x-ray emission plotted against target atomic number, and (c) x-ray conversion efficiency as a function of target atomic number as given in Ref. 22, for comparison.

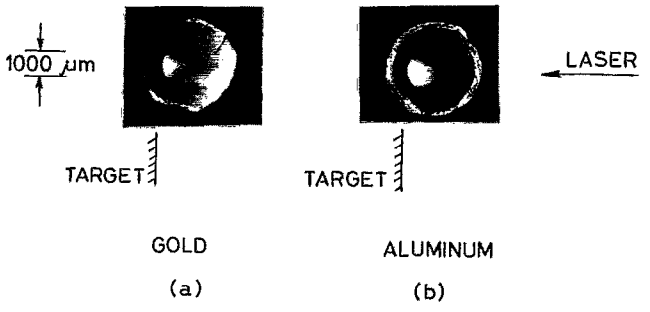

FIG. 4. Time-integrated x-ray pinhole picture for (a) gold target and (b) aluminum target at a laser intensity of 5×10^{12} W/cm^2.

the plasmas measured using a differential x-ray calorimeter against target atomic number. The incident laser intensity was 5×10^{12} W/cm^2. All shadowgrams were recorded 7 nsec after the main laser pulse. We find that molybdenum and gold are nearly at the peak of the x-ray emission plot and so is the corresponding plasma jet density. On the other hand, lead, tantalum, tin, and titanium show lower radiation losses and they also show a much less pronounced plasma jetting. Plastic, magnesium, and aluminum exhibit very much lower radiation losses as compared to molybdenum and gold. These materials show a total absence of plasma jetting. We have also compared the measured dependence of x-radiation losses (as a function of target atomic number) with other authors[22] and find a reasonable agreement as far as relative positions of maxima and minima are concerned, as shown in Fig. 3(c). A time-integrated x-ray pinhole picture of a gold target recorded with a 25 μm diam pinhole and an aluminized polycarbonate foil as a filter is shown in Fig. 4(a). The overall magnification in the pictures was 5×. The formation of a single jet of diameter 50–70 μm in the corona about 1 mm from the target is clearly observed. The length of this jet is about 700 μm measured from a distance of about 1 mm from the target surface. The x-ray pinhole picture for aluminum [Fig. 4(b)] shows no plasma jets.

Figures 5(a) and 5(b) show the interferograms of the gold plasma at a laser intensity of 2.5×10^{12} W/cm^2 and 10^{13} W/cm^2, respectively. The irradiation spot diameter was 160 μm, and the probe pulse to main pulse delay was 8 nsec. It is seen that at lower intensity the jet dimensions are nearly as large as 50–70 μm, where at higher intensity they decrease to below the resolution limit and a complete smearing of interference fringes 300–500 μm away from the target surface is observed. In Figs. 5(a) and 5(b) it is seen that there appears a severe curving in of fringes in the regions of the jets since the displacement of the lower-order fringes takes place in the plasma region due to a decrease of refractive index as a result of increase in electron density. Calculations show that in these regions electron density is at least 5–10 times higher than in the surrounding plasma regions. When the laser intensity is further increased to about 2×10^{13} W/cm^2 by focusing the laser beam to a 30 μm diam spot on the target, interference fringes cannot be seen up to a distance as large as 800 μm, as seen in Fig. 5(c). This could be due to the disruption caused by several very fine jets which are beyond the resolution limit. Figure 6 shows the plot of plasma jet dimensions with laser intensity in a gold target. It is generally observed that at laser intensities greater than 10^{13} W/cm^2, the jet dimensions decrease beyond the resolution limit of our experiments. This observation can be explained on the basis of an argument that an increase of laser intensity results in a higher plasma temperature accompanied by a smaller τ_{th}. Thus the increased thermal smoothing dictates a smaller scale length of plasma jets. Figure 7 shows the shadowgram of a 10 μm thin gold coated zapon recorded 14 nsec after the peak of the laser pulse. Jets are clearly seen on the rear side also.

Plasma expansion velocity was measured using a Langmuir probe for a molybdenum target ($Z = 42$) at two different intensities, namely 10^{13} W/cm^2 and 2×10^{13} W/cm^2. The velocity was, respectively, 1.15×10^7 and 1.34×10^7

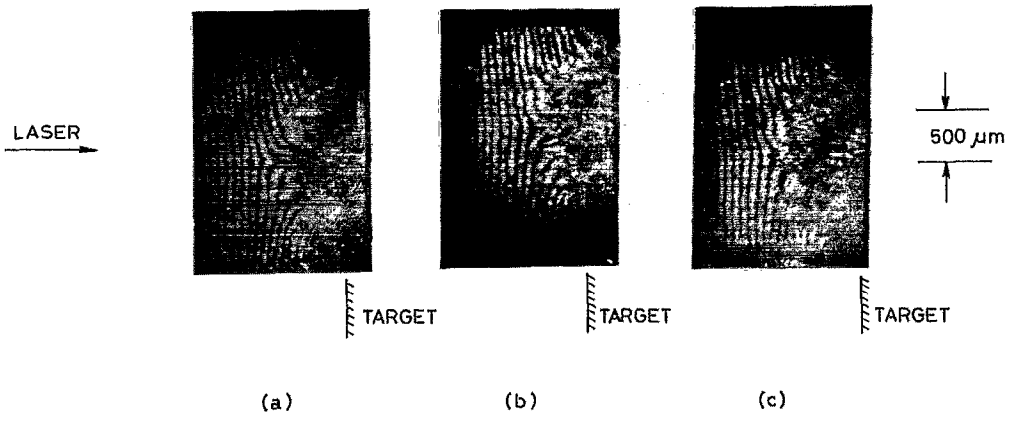

FIG. 5. Inteferograms of a gold plasma recorded 8 nsec after peak of main laser pulse at a laser intensity (a) 2.5×10^{12} W/cm^2, (b) 10^{13} W/cm^2, (c) 2×10^{13} W/cm^2.

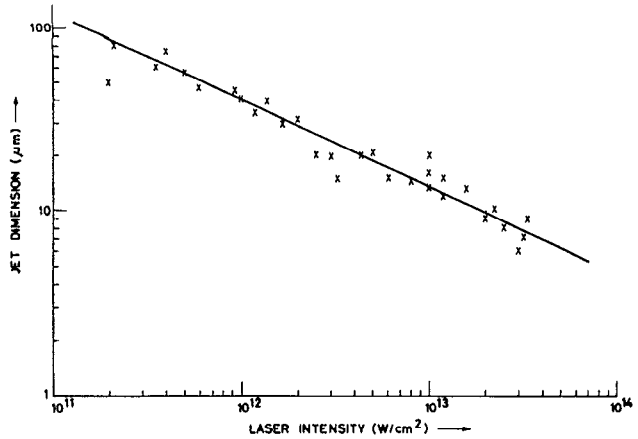

FIG. 6. Variation of jet dimensions with laser intensity on a gold target.

cm/sec, and is thus seen to scale as predicted by theory, in spite of the fact that strong jetting was observed at the lower intensity. Ablation pressure measured at these laser intensities also showed scaling as predicted by theory accompanied by a uniform foil motion. Our earlier experiments[5] on the time evolution of plasma jetting as well as the present experiments therefore indicate that plasma jets are formed after the ablative acceleration phase and thus do not affect ablation parameters such as pressure, plasma expansion velocity, mass ablation rates, and also uniformity of target motion.

V. CONCLUSIONS

The experimental results and the analytical model strongly indicate the formation of plasma jets in targets characterized by high radiative losses. Plasma jets occur due to the growth of radiative cooling instabilities in the low-density plasma corona. The model explains the various conditions under which this instability can grow. The presence of strong jetting on the rear side also strongly indicates this instability when a plasma freely expands in vacuum after the laser pulse is over. Increased electron density and x-ray emission from the region of plasma jets is a supportive indication of a radiative cooling instability. We can say that, though in the present experiments the plasma jets do not adversely affect the hydrodynamic stability of foil targets, in reactor grade pellets one can envisage some problems. Plasma jets formed in the long scale length plasmas in reactor grade pellets can become precursors for filamentation in the later part of the laser pulse causing a deterioration in laser–plasma coupling. In cannonball-type targets,[23] plasma jets formed inside the gold cavity can result in nonuniform implosion of the pellet. Also, x-ray laser schemes could be adversely affected due to the plasma nonuniformity caused by jets.

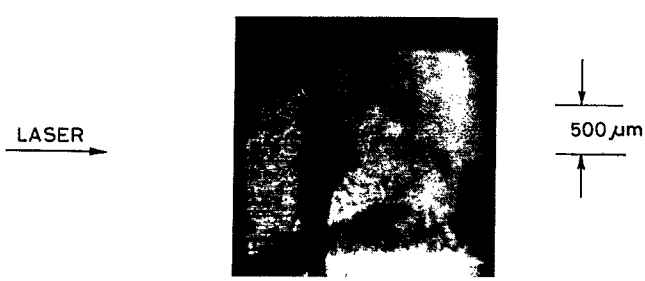

FIG. 7. Rear side shadowgram of a 10 μm thin gold coated foil recorded 14 nsec after the peak of laser pulse. Plasma jets are observable on the rear side of the foil.

ACKNOWLEDGMENTS

The authors wish to thank Dr. H. C. Pant and T. Desai of the Laser and Plasma Technology Division and Dr. S. V. Lawande, M. K. Srivastava, and H. D. Parab of the Theoretical Physics Division of Bhabha Atomic Research Centre for stimulating discussions. M. Khan, S. Sarkar, and B. Chakraborty acknowledge a useful discussion with Dr. M. R. Gupta and Dr. K. P. Das of the Applied Mathematics Department, Calcutta University. U. K. Chatterjee, Head, Laser and Plasma Technology Division is acknowledged for his constant encouragement.

This work has been partly supported by Board of Research in Nuclear Science, Government of India.

[1]O. Willi and P. T. Rumsby, Opt. Commun. **37**, 45 (1981).
[2]J. A. Stamper and B. H. Ripin, Phys. Rev. Lett. **34**, 138 (1975); J. A. Stamper, E. A. Mclean, and B. H. Ripin, Phys. Rev. Lett. **40**, 1177 (1978); G. Thiell and B. Meyer, Laser Part. Beams **3**, 51 (1985).
[3]M. J. Herbst, R. R. Whitlock, and F. C. Young, Phys. Rev. Lett. **47**, 91 (1981).
[4]S. Denus, H. Fiedorowicz, S. Nagraba, W. Pawlowicz, L. Sulwinski, A. Wilczynski, and J. Wolowski, Opt. Commun. **47**, 127 (1983).
[5]L. J. Dhareshwar, P. A. Naik, P. D. Nandwana, and H. C. Pant, J. Appl. Phys. **61**, 4458 (1987).
[6]O. Willi, P. T. Rumsbi, and S. Sartang, IEEE J. Quantum Electron. **QE-17**, 1909 (1981).
[7]Z. Q. Lin, O. Willi, and P. T. Rumsby, J. Phys. D Appl. Phys. **14**, L35 (1981).
[8]O. Willi, P. T. Rumsby, C. Hooker, A. Raven, and Z. Q. Liu, Opt. Commun. **41**, 110 (1982).
[9]H. Hora, Phys. Fluids **17**, 939 (1974).
[10]C. E. Max, Phys. Fluids **19**, 74 (1976).
[11]E. F. Gabl, B. H. Failor, C. J. Armentrout, N. D. Delamater, W. B. Fechuer, R. A. Bosch, G. E. Bush, Z. M. Koenig, D. Ress, L. Suter, and R. J. Schroeder, Phys. Rev. Lett. **63**, 2737 (1989).
[12]Z.-Z. Xu, S.-S. Chen, L.-H. Lin, Z.-M. Jian, W.-G. Zhang, and A.-D. Qian, Phys. Rev. A **39**, 808 (1989).
[13]Z.-Z. Xu, Z.-M. Jiang, L.-H. Lin, S.-S. Chen, Z.-Q. Zhang, and P.-Z. Fan, Opt. Commun. **69**, 49 (1988).
[14]R. C. Evans, J. Phys. D Appl. Phys. **14**, 173 (1981).
[15]D. A. Tidman and R. A. Shanny, Phys. Fluids **17**, 1207 (1974).
[16]M. G. Haines, Phys. Rev. Lett. **47**, 917 (1981).
[17]H. Puell, Z. Naturforsch. **15a**, 1807 (1970).
[18]J. W. Dawson, *Laser Plasmas and Nuclear Energy*, edited by H. Hora (Plenum, New York, 1975), p. 199.
[19]E. A. Routh, *The Advanced Part of a Treatise on the Dynamics of a System of Rigid Bodies Part-II* (Macmillan, London, 1970), p. 1884.

[20]G. Thiell and B. Meyer, Laser Part. Beams **3**, 51 (1985).
[21]J. C. Moreno, S. Goldsmith, H. R. Griem, L. Cohen, R. Epstein, D. Bradley, P. A. Jaanimagi, and J. Knauer, Phys. Rev. A **40**, 4564 (1989).
[22]C. Yamanaka, H. Azechi, E. Fujiwara, S. Ido, Y. Izawa, T. Jitsuno, Y. Kato, Y. Kitagawa, K. Mima, N. Miyanaga, T. Mochizuki, S. Nakai, M. N. Nakatsuka, H. Niki, H. Nishimura, K. Nishihara, T. Norimatsu, T. Sasaki, S. Sakabe, T. Yabe, M. Yamanaka, T. Yamanaka, and K. Yoshida, *Twenty Years of Plasma Physics*, edited by B. McNamara (World Scientific, Philadelphia, 1984), p. 163.
[23]H. Shiraga and Y. Kitaygawa, Institute of Laser Engineering, Osaka University Quarterly Progress Report on Fusion Programme, Osaka, ILE-QPR-84-10, 1984, p. 7; H. Azechi, Jpn. J. Appl. Phys. **20**, L477 (1981).